Theoretical investigations of quantum walks by cold atoms in a double optical lattice

Nandan Satapathy,[1,*] Henning Hagman,[2] Martin Zelán,[2] Anders Kastberg,[2] and Hema Ramachandran[1]
[1]*Raman Research Institute, Sadashivnagar, Bangalore 560 080, India*
[2]*Department of Physics, Umeå University, SE-90187 Umeå, Sweden*
(Received 24 February 2009; published 1 July 2009)

We investigate the feasibility of carrying out quantum walks with cold atoms in a double optical lattice. Monte Carlo simulations of time-of-flight (TOF) detection and absorption imaging were carried out, focusing on a specific experimental implementation. These indicate that absorption imaging would be best suited for detection of quantum walks. With typical experimental parameters a few hundred quantum walk steps will be needed for an unambiguous detection of the quantum walk signature. We show that in special cases, few-step quantum walks can also be detected in our system if one measures the relative population of the atoms in their internal states rather than their displacement in space, that is, measurements are made in the space of the coin operator rather than in that of the displacement operator.

DOI: 10.1103/PhysRevA.80.012302 PACS number(s): 03.67.Lx, 37.10.Jk

I. INTRODUCTION

The concept of a quantum walk has evoked considerable research interest in quantum information [1] in recent times, particularly as a possible mechanism for quantum search algorithms [2–5]. In a classical one dimensional random walk, a particle starting from the origin moves either to the right or to the left depending on the outcome of the toss of a coin. The quantum analogy also considers the displacement of a particle conditioned on the outcome of the toss of a coin, with the distinction that on being tossed, the coin goes into a superposition of states leading to a superposition of displacements and thus a spread in the wave function of the quantum particle. Coherence of the wave function permits quantum interference of displacement amplitudes of the particle in subsequent steps leading to probability distribution functions quite different from the classical case. For example, N steps of a classical random walk by a particle starting from the origin results in a Gaussian probability distribution of positions, centered around the origin and a standard deviation proportional to $\sqrt{N}$. In contrast, a quantum walk starting from the origin results in a position probability distribution peaking away from the origin with the peak displacement and standard deviation increasing as N. This is the reason why quantum search algorithms based on quantum walks are expected to be faster than their classical counterparts.

In the case of light, quantum walks have been proposed based on the polarization states [6–8] and on the orbital angular momentum of a single photon [9]. In the case of matter, schemes have been devised on trapped ions [10], ultracold atoms in optical lattices [11], Bose-Einstein condensate (BEC) [12], optical trap arrays [13], cavity quantum electrodynamics (QED) [14], externally driven cavities [15], Rydberg atoms in a cavity [16], and Rydberg atoms in optical lattices [17]. While numerous proposals exist, a few implementations of quantum walk have also been reported. The first practical implementation of a quantum walk was of the continuous kind [18] by Du *et al.* [19] in a two-qubit liquid NMR system. Ryan *et al.* [20] implemented a discrete time quantum walk on a square using a three-qubit liquid state NMR system. Discrete quantum walks on a line have also been demonstrated with photons using linear optical elements by Do *et al.* [21] and Zhang *et al.* [22]. Recently, Perets *et al.* [23] have realized a large scale continuous quantum walk using photons in waveguide lattices. Implementations of quantum walks have proved to be a challenging task and in case of discrete quantum walks, only up to three steps of quantum walk have been reported to our knowledge. Factors such as rapid decoherence of the system, inefficiency of the processes involved in making a quantum step, and scaling up requirements have been major issues.

In this paper we focus on discrete quantum walks by cold atoms (nondegenerate) in a double optical lattice. Using methods of Monte Carlo simulations we critically examine and conclude that it would indeed be possible for a quantum walk of a few hundred steps to be unambiguously detected by standard absorption imaging techniques for realistic experimental parameters in our system. Furthermore, we show that in special cases, even a few-step quantum walk can be detected in spite of the fact that each step size of the walk is few orders of magnitude smaller than size of cold atom sample.

In the following sections, we begin by a short introduction to discrete quantum walks and their salient features. Next we give a description of the proposed experimental procedure for performing quantum walks with cold atoms in a double optical lattice and detection techniques that may be employed. This is followed by a description of the Monte Carlo model used to simulate the walk. We then proceed to discuss the results of our Monte Carlo simulations and also examine the effect of experimental inefficiencies and decoherences on the quantum walk. Finally we describe how we can detect a few-step quantum walk.

II. DISCRETE QUANTUM WALKS

Let us consider a particle described by a wave function $\Psi_i=\Sigma_{k,s}\phi(k,s)$, where i denotes the ith step of the walk, k denotes the position, and s the internal state. The position k

*nandan@rri.res.in

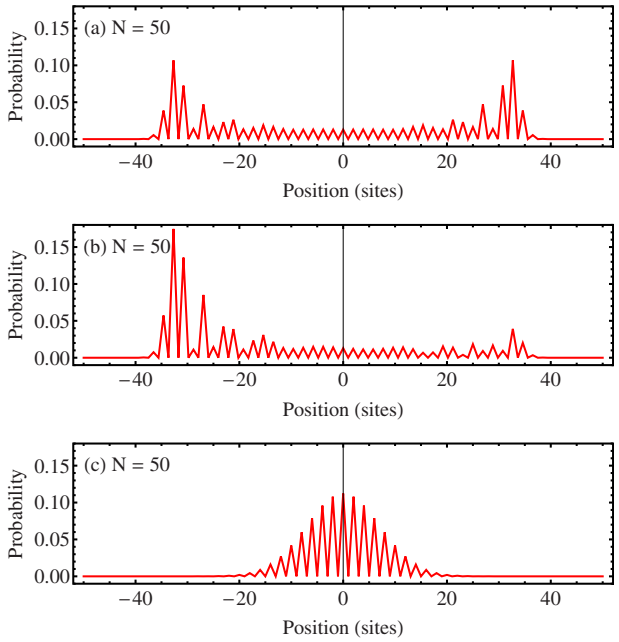

FIG. 1. (Color online). Probability versus displacement for (a) symmetric quantum walk, (b) asymmetric quantum walk, and (c) classical random walk. In all cases, the number of steps, N equals 50.

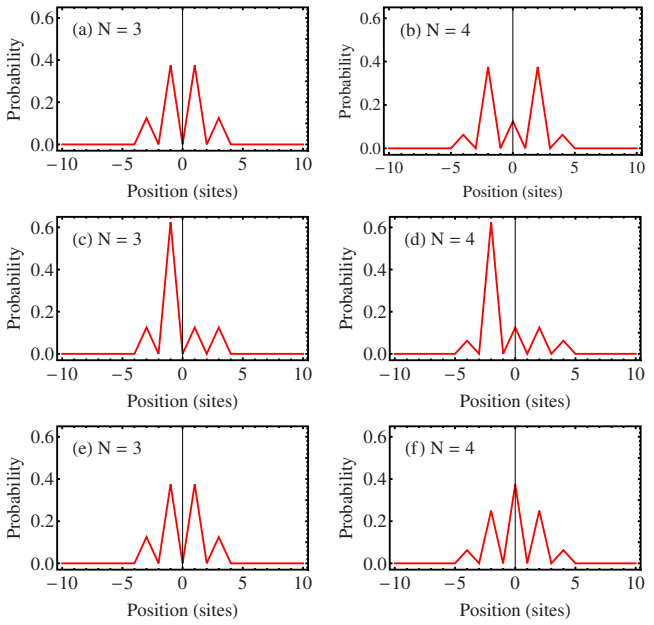

FIG. 2. (Color online). Probability versus displacement (a and b) for symmetric quantum walks, (c and d) for asymmetric quantum walks, and (e and f) for classical random walks. In all cases, the panel on the left is for a 3-step walk and the one on the right a 4-step walk.

can take discrete values from $-\infty$ to ∞ and s can have one of the two values X or Y. The operator H defined below, which puts each internal basis state into a superposition state, simulates the toss of the quantum coin. The operator D is the conditional displacement causing a translation to the right or to the left depending on the internal state (X,Y).

$$H[\phi(k,X)] \rightarrow \phi(k,X+Y)$$

$$H[\phi(k,Y)] \rightarrow \phi(k,X-Y)$$

$$D[\phi(k,X)] \rightarrow \phi(k+1,X)$$

$$D[\phi(k,Y)] \rightarrow \phi(k-1,Y)$$

An application of the sequence DH constitutes a single step of the quantum walk. Beginning with $\Psi_0=\phi(0,X)$, the wave function after N steps is given by,

$$\Psi_N = (DH)\Psi_{N-1} = (DH)(DH)\Psi_{N-2} = \ldots . = (DH)^N\Psi_0.$$

The H operator considered here is Hadamard operator which puts states X and Y into equal superposition. In general one can put the states into any arbitrary superposition and repeat the process. In this paper, we shall be considering only the Hadamard operator.

We now briefly mention some well-known features of quantum walks. In Fig. 1(a) we give the probability distribution after a 50-step quantum walk in position space for a single atom starting in state $X+iY$ from the origin. This gives a symmetric distribution. On the other hand, if the particle starts off in the state X or the state Y, an asymmetric walk results [Fig. 1(b)]. However, in both the symmetric and the asymmetric cases, the peak of the probability distribution is displaced away from the origin. In contrast, a classical random walker remains centered at the origin, but with an increased spread [Fig. 1(c)]. In principle, right from the third or fourth step onwards quantum walks and classical walks can be distinguished from one another as seen in Fig. 2.

III. QUANTUM WALK IN A DOUBLE OPTICAL LATTICE

A. Experimental description

The quantum walker we consider is a cesium atom, which has two hyperfine ground states, namely, $6s\ ^2S_{1/2}$, $F=3$ and $6s\ ^2S_{1/2}$, $F=4$, which are separated by 9.2 GHz [24]. In an experiment, the atoms are first collected and cooled in a magneto-optical trap and then loaded into a double optical lattice [25,26]. The double optical lattice consists of two sets of spatially overlapped lattice beams in a three-dimensional generalization of the lin$\perp$lin configuration [see Fig. 3(a)] [27,28]. This generates a lattice topography which is insensitive to phase fluctuations in the lattice beams. The two sets of laser beams operate at the $F=3\rightarrow F'=4$ and the $F=4\rightarrow F'=5$ transitions within the $D2$ transition lines that couple $6s\ ^2S_{1/2}$ ground levels to $6p\ ^2P_{3/2}$ levels. They can be red detunined up to about 1 GHz [see Fig. 3(b)]. Thus, each of the two interpenetrating optical lattices preferentially traps atoms in one of the hyperfine ground states—the former traps atoms in the $6s\ ^2S_{1/2}$, $F=3$ and the latter those in $6s\ ^2S_{1/2}$, $F=4$. In general, higher detunings of the lattice beams increase the coherence time. However, with the current experimental configuration [29], the detunings have to be sufficiently small compared to the hyperfine splitting of the ground states in order not to couple both transitions.

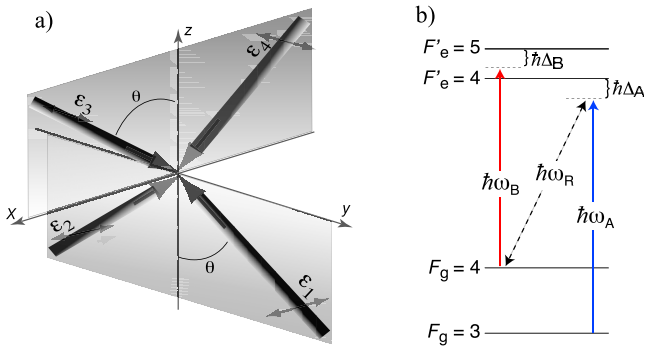

FIG. 3. (Color online). (a) The three-dimensional generalization of the lin ⊥ lin configuration that creates the double optical lattice. ϵ denotes the different polarization directions for the different lattice beams and θ is the angle between the lattice beams and the z axis. (b) The energy diagram of the hyperfine D2 transition lines which are considered in this paper. A and B represent the lattice beams and R the Raman beam, ω denotes the angular frequency of the beams and Δ the detuning.

The wavelengths of the two lattice beams differ by less than ~picometer and so over the region of the cold cloud, the lattice sites of the two optical lattices can be made coincident. Atoms trapped in the two optical lattices can be moved with respect to one another by introducing a relative spatial phase shift between the double optical lattices. This is achieved by controlling the phases in the lattice beams by changing the optical path length of one set of lattice beams e.g., with an electrooptical modulator (EOM) [26]. It may be noted here that during translation, the topography the optical lattice does not change. A shift of the relative spatial phases by 2π would then act as a D operator.

When the two lattices are coincident, one may cause a coherent population transfer between the ground states by means of an additional Raman laser beam [see Fig. 3(b)] tuned to the $6s\ ^2S_{1/2},\ F=4 \rightarrow 6p\ ^2P_{3/2},\ F'=4$ transition. (To be two-photon resonant with the Raman transition it should have the same detuning that the lattice beam A has). This would result in a concomitant transfer of atoms from one lattice to the other. By denoting the two hyperfine ground states, $6s\ ^2S_{1/2},\ F=3$ and $6s\ ^2S_{1/2},\ F=4$ as the coin states X and Y, we can utilize the Raman transition to set an arbitrary initial state, $aX+bY$. A Raman $\pi/2$ pulse would constitute the H operator.

The initial cloud of atoms in the double optical lattice has a size of the order of a millimeter and temperatures in range of few microkelvin depending on the potential depth [30,31]. The lattice spacing in the vertical direction is $\lambda/\sqrt{2}$ (~0.5 μm), which will determine the spatial step length of the D operator.

B. Detection techniques

The two most commonly used techniques for detection of cold atoms are time-of-flight (TOF) and direct imaging (absorption imaging). In the former case atoms are released from the lattice and allowed to fall freely under gravity spreading due to the velocity distribution. The falling atoms are intercepted by a probe beam, where they fluoresce. From the recorded fluorescence signal one may infer the velocity and position distribution of the atoms [32,33]. Two factors, the initial positional spread of the collection of atoms and their temperature (the latter leading to a velocity spread in the collection of atoms) limit the resolution achievable. In the case of absorption imaging, a beam of light is passed through the collection of atoms and the transmitted light is recorded. Attenuation of the beam is indicative of intervening atomic population.

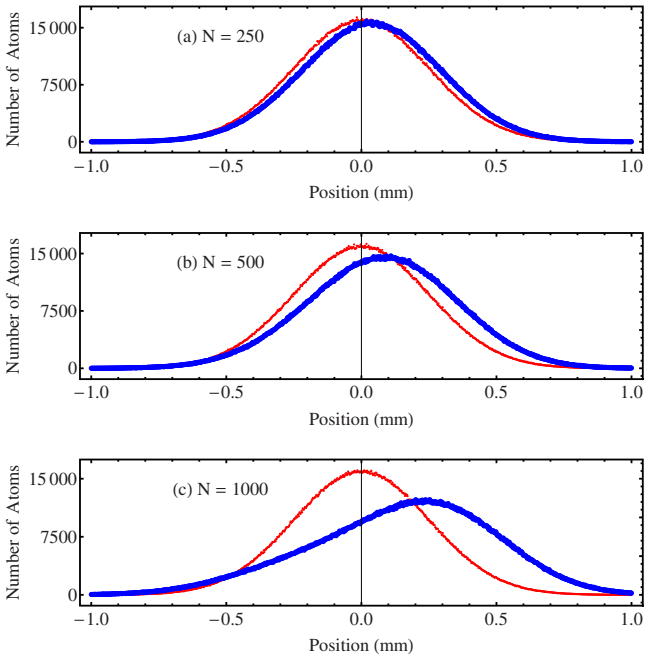

FIG. 4. (Color online). Simulated absorption signal after classical random walk [red (thin) curve] and asymmetric quantum walk [blue (thick) curve] of (a) 250 steps, (b) 500 steps, (c) 1000 steps in a cold cloud of size 1 mm.

C. Monte Carlo model

We carried out Monte Carlo simulations of direct imaging and of TOF method to study the feasibility of detection of quantum walks in such a collection of atoms in cold cloud. Atoms in the cold cloud have a Gaussian spatial distribution and a Maxwellian velocity distribution. We considered ten million noninteracting atoms. Each atom is assigned a random position in a three-dimensional space (x,y,z coordinates) weighted by a Gaussian probability distribution. The size of the cloud is taken to be twice the full width at half maximum of the Gaussian probability distribution. For the TOF method, each atom is also assigned a random velocity weighted by Maxwell-Boltzmann distribution corresponding to a given temperature.

The probability distribution for N-step quantum walk was determined using a recursion formula for the walk. For each atom a weighted random number was generated, with the N-step distribution generated above used for weighting. This random number multiplied by the lattice spacing was added to the initial z coordinate of the atom to obtain the final

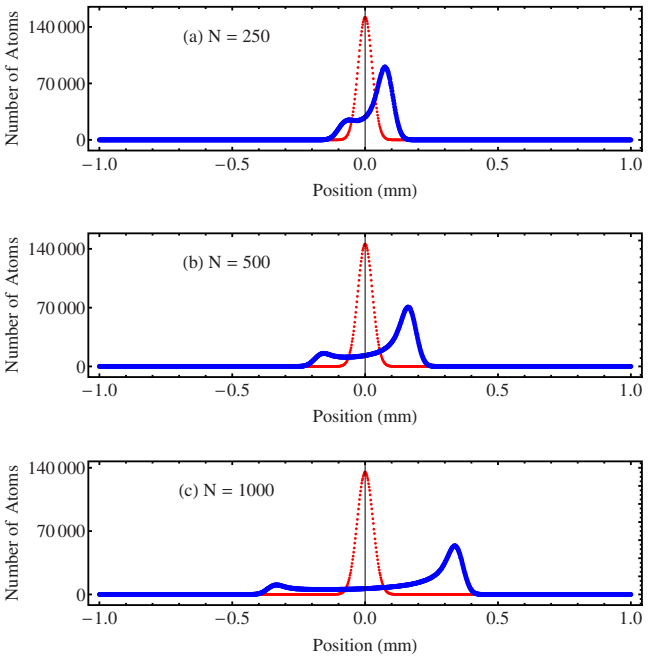

FIG. 5. (Color online). Simulated absorption signal after classical random walk [red (thin) curve] and asymmetric quantum walk (blue/thick curve) of (a) 250 steps, (b) 500 steps, (c) 1000 steps in a cold cloud of size 0.1 mm.

position of the atom. Note that the one-dimensional walk is performed in the (vertical) z direction and the x and y coordinates remain unchanged. In this manner we obtained the positional distribution of atoms in the cold cloud, having performed an N-step quantum walk.

We simulated a direct absorption imaging signal for an imaging beam sent along the y direction by summing over the position coordinate y. We also summed over the position coordinate x to get the distribution of atoms along the z direction after the quantum walk. Histograms were thereafter formed by binning the z positions with a bin size depending on the resolution of the imaging optics and the charge coupled device camera.

For simulating the TOF signal, the time of arrival of atoms, upon release from the trap, at a probe beam placed at a distance d vertically below the cloud, was calculated for each atom using its z position after the N-step quantum walk and its initial velocity. A histogram was formed by binning these times of arrivals using a bin size appropriate for the experimental setup. In this case the time bin was 10 μs.

Both the absorption and TOF signals thus generated are compared with the signals simulated for a N step classical walk for a collection of cold atoms in an optical lattice for the same parameters [shown as the red (thin) curve in the Fig. 4–7]. In the classical case the final probability distribution remains Gaussian.

IV. RESULTS OF MONTE CARLO SIMULATIONS

A. Simulated absorption imaging

The simulated absorption signals are given in Fig. 4 for an atom cloud of 1 mm diameter undergoing 250, 500, and 1000

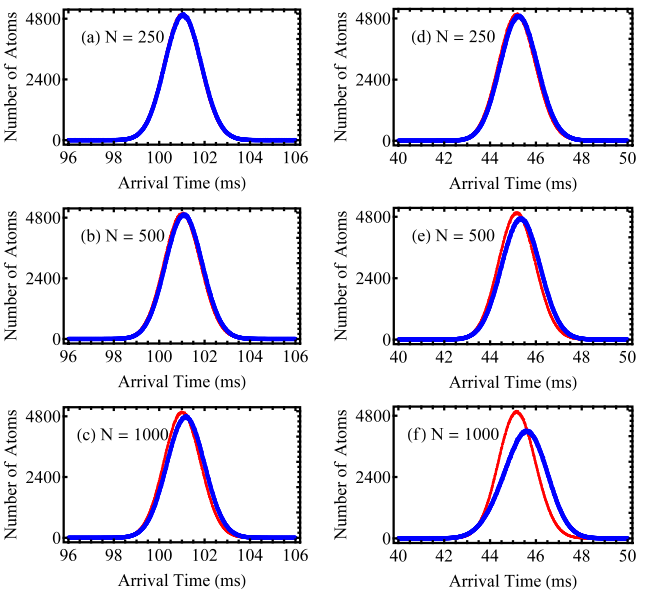

FIG. 6. (Color online). Simulated TOF signals for cloud of 0.1 mm at 1 μK with probe placed [(a)–(c)] 5 cm and [(d)–(f)] 1 cm below the cloud for various N-step walks. In each panel, the red (thin) curve corresponds to a classical walk and the blue/thick curve to an asymmetric quantum walk.

steps of asymmetric quantum walks, where each step size is $\lambda/\sqrt{2}$. It is seen that careful measurements can enable distinction between a classical and a quantum walk even for 250 steps. However no striking departure from a Gaussian probability distribution of positions is evident even for 1000 steps, though there is a slight displacement of the center of mass of the collection of atoms. This is understandable as the maximum possible displacement of an atom even in 1000

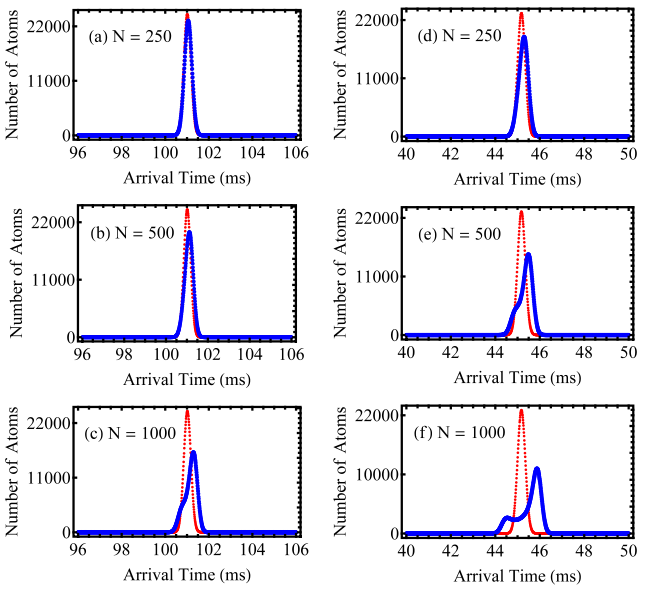

FIG. 7. (Color online). Simulated TOF signals for cloud of 0.1 mm at 200 nK with probe placed [(a)–(c)] 5 cm and [(d)–(f)] 1 cm below the cloud for various N-step walks. In each panel, the red (thin) curve corresponds to a classical walk and the blue/thick curve to an asymmetric quantum walk.

step case lies within the initial size of the cloud. Figure 5 shows the same for a cloud of size 0.1 mm. In this case, the typical features of a quantum walk, namely, the suppression of the positional probability distribution at the center and the peaking at the ends, is very clearly seen even at 250 steps. This is even more pronounced for 500 and 1000 step walks.

B. Simulated time of flight detection

Our results from the simulation of the TOF method are now discussed. This measurement technique was considered because of the good signal to noise ratio it offers [33]. Figures 6 and 7 are the simulated TOF signals for atom clouds of 0.1 mm size at 1 μK and 200 nK respectively. In each figure the first column shows the TOF signal for a probe beam sent 5 cm below the cloud and the second column for a probe beam 1 cm below the cloud. In each of the columns, the first row shows the result of an asymmetric quantum walk after 250 steps, the second after 500 steps, and the third after 1000 steps. Unlike the case of absorption imaging where the temperature of the cloud does not affect the measurement, the TOF signal is very sensitive to this parameter; in fact the TOF technique is used to measure the temperature (velocity distribution) of a cold cloud. Thus, it is not surprising that the TOF signal for the 1 μK case is quite different from the one for the 200 nK case.

Also, the distance of the probe beam from the cloud is an important factor—too distant a beam would allow the masking out of the effects of a quantum walk by the ballistic spread of atoms during their flight. We see from Fig. 6 that a temperature of 1 μK is too high to bring out the characteristic features of the quantum walk. However, a quantum walk can indeed be distinguished from the case of a classical walk when the probe is placed sufficiently close as is seen from Figs. 6(e) and 6(f). The signal however remains essentially a Gaussian though somewhat skewed. The case of the atom cloud at 200 nK (Fig. 7) shows the characteristic quantum walk features after a large number of steps (1000) in the case of a distant (5 cm) probe beam and for about 500 steps for the case of probe beam 1 cm below the cloud. Comparison of Figs. 5–7 shows that absorption imaging technique is better suited for detecting and measuring quantum walks as the velocity spread (temperature) of the atoms is an irrelevant parameter here.

So far we have seen that for atoms in typical cold atomic cloud a few hundred steps are needed to be carried out in order for the features of quantum walk to be observed. However, this coupled with imperfect Raman transfers, inefficient physical displacements, and decoherence due to spontaneous emissions may severely constrain practical implementation. This aspect will be discussed next section.

V. INEFFICIENCIES AND DECOHERENCE IN QUANTUM WALKS

A. Inefficient quantum walk

The quantum walks described and performed in Monte Carlo simulations assume perfect Hadamard and displacement operators. In practical implementations there are serious considerations. One of the inefficiencies that may arise is that some atoms are not moved to their neighboring lattice sites during the displacement operation but remain at their current sites. As a result the spread of atom slows down with respect to number of steps N of quantum walk. At the end of a N-step quantum walk with an inefficient displacement operator, the atom is in a weighted sum of all possible k-step quantum walks, with k extending from one to N. This can be seen in Fig. 8 which gives the positional probability distribution of an atom after 250 steps of quantum walk for various efficiencies of the displacement operator. The walk depicted in (a) has largest spread; it represents a Hadamard walk with 100% efficiency of the displacement operator. In this curve, alternate sites have zero probability for finding an atom characteristic of discrete walks. All the other curves, which represent Hadamard walks with various reduced displacement fidelities have a finite nonzero probability at all sites between the two extremes. Also, the most probable (peak) displacement occurs closer to the center with decreasing fidelity of the displacement operator.

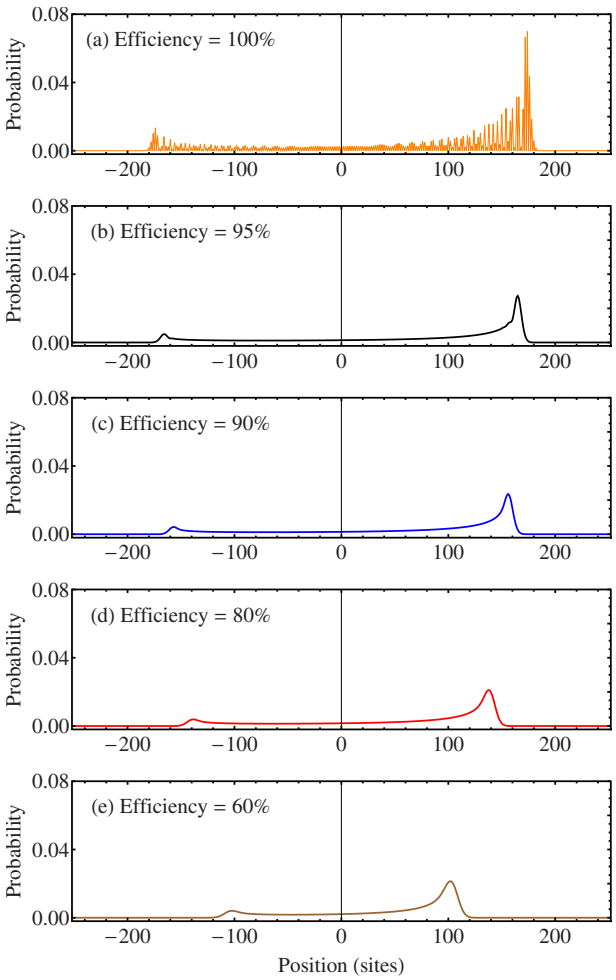

FIG. 8. (Color online). Positional probability distributions after 250-step asymmetric quantum walks of different efficiencies of the displacement operator.

However, this does not imply classical random walk nature. In a classical random walk, the probability distribution remains peaked at the origin and the standard deviation of

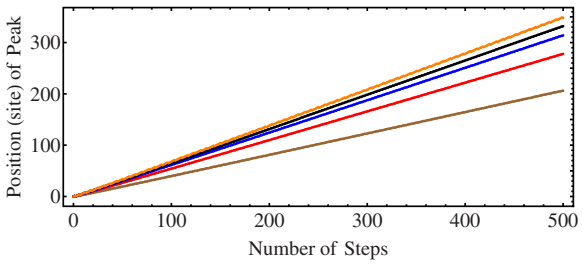

FIG. 9. (Color online). The most probable (peak) displacement versus the number of steps of asymmetric quantum walks for different efficiencies of displacement operator. Lines shown from top to bottom represent 100 (orange), 95 (black), 90 (blue), 80 (red), and 60% (brown) efficiency of the displacement operator respectively.

the displacement probability varies as $\sqrt{N}$, N being the number of steps. The ideal quantum walk on the other hand is known to have a standard deviation linear in N [1]. We examined the most probable displacement for various reduced fidelities of displacement operator. The results are shown in Fig. 9, where the position of the most probable displacement is plotted as a function of N. It is seen that the most probable displacement remains linear with the number of steps of the asymmetric quantum walk though the slope reduces with decreasing fidelity of the displacement operator. Given in Fig. 10 are the absorption images corresponding to the probability distributions of Fig. 8 assuming a cold cloud of 0.1 mm size in a double optical lattice. It is seen that even for as low as 80% efficiency and to a certain extent even for 60% efficiency, a 250-step walk gives a good quantum walk behavior in the absorption imaging.

B. Decoherence

Spontaneous emissions during Raman pulse cycles and the inherent scattering in the optical lattices contribute to decoherence in our system. In our simulation, decoherence was modeled in the following manner. For a coherence of $Q\%$, an atom during the Hadamard operation was taken to perform a $\pi/2$ Rabi cycling and go into a superposition state with a probability $Q\%$. With a probability $(100-Q)\%$, atoms were assumed to undergo spontaneous emission and collapse to one of the lattice sites with a spatial probability distribution that the atomic wave function had just prior to the Hadamard operation and with equal probability of going to states X or Y. Thereafter, the atom starts a fresh quantum walk. By repeating the process for about a million times we get average position probability distribution of an atom after N steps of a quantum walk with coherence of $Q\%$.

Figures 11 and 12 show the position probability distribution after 50 and 250 steps quantum walk with various reduced coherences. It should be noted that alternate sites have probability zero; this is inherent to a discrete walk and is not an interference phenomenon. The alternate sites with probability zero have been omitted in the plot for better representation. It can be seen from Fig. 11(d) that a 50-step quantum walk with 95% coherence (where there is 5% chance of atoms to decohere at each step) begins to resemble the classical random walk. For a 250-step walk this happens for 99% [Fig. 12(c)]. For reduced coherences of 90 and 80% the classical nature is even more apparent as the probability distribution becomes Gaussian; however, the width is still large compared to the completely classical random walk. Absorption images corresponding to the probability distributions of Fig. 12 assuming a cold cloud of 0.1 mm size in a double optical lattice are given in Fig. 13.

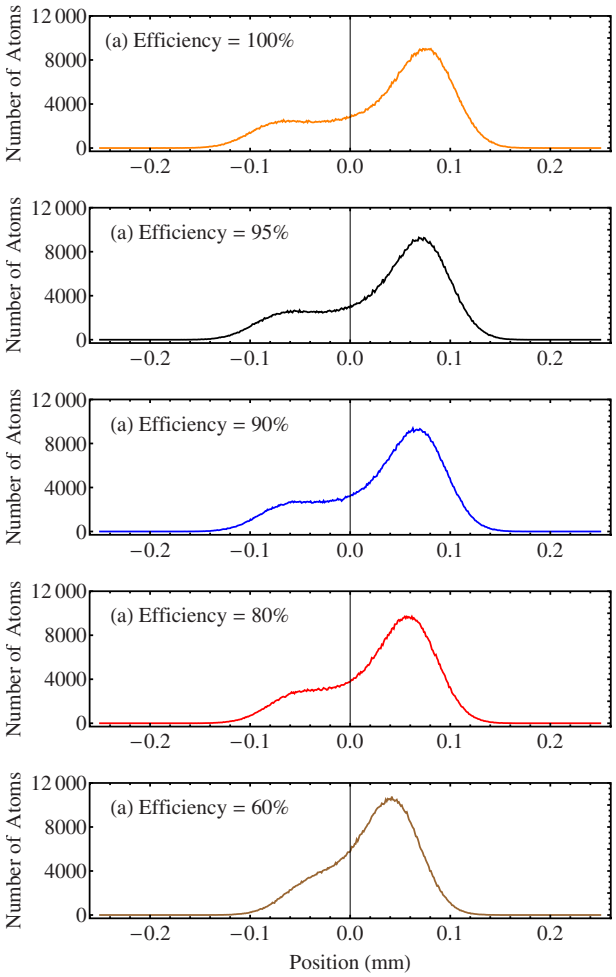

FIG. 10. (Color online). Simulated absorption signal of asymmetric quantum walks of 250 steps for different efficiencies of displacement operator.

From the discussions so far, the following emerges. On the one hand, a large number of steps can be required for an unambiguous detection of the typical signature of a quantum walk, namely, suppressed positional probability at the origin and its peaking toward the periphery. This requirement may increase further due to inefficient displacement operations. At the same time, the decoherence in the system can rapidly wash out the quantum walk features and thus restrict the number of steps that may be implemented. To provide a more complete picture, it is vital to find alternative methods that can work for quantum walks with just a few steps. We discuss this in the next section.

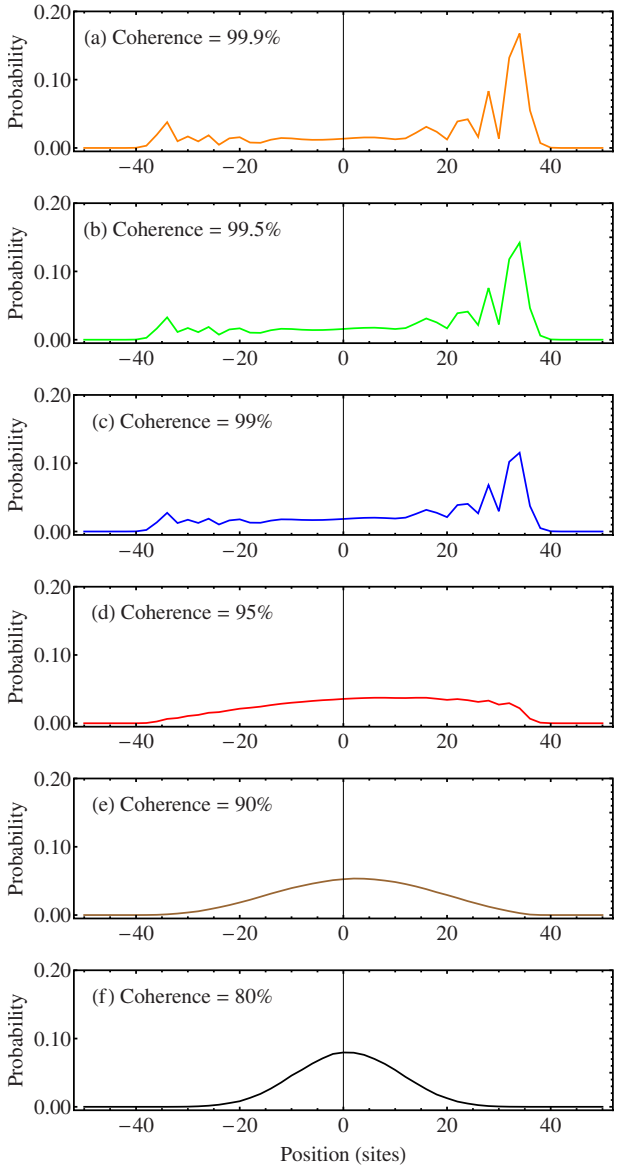

FIG. 11. (Color online). Positional probability distribution for asymmetric quantum walk of 50 steps for different coherences. Alternate sites that have zero probability have been omitted for clarity.

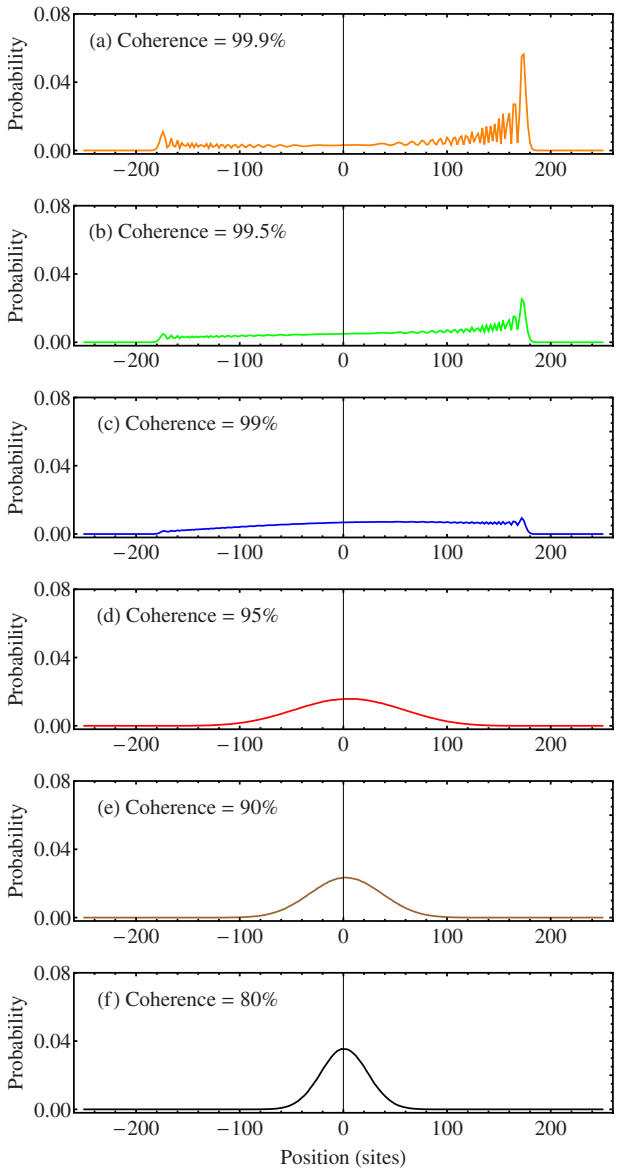

FIG. 12. (Color online). Positional probability distributions for asymmetric quantum walk of 250 steps for different coherences. Alternate sites that have zero probability have been omitted for clarity.

VI. DETECTION OF A FEW-STEP QUANTUM WALK: PROJECTION INTO INTERNAL STATE SPACE

We now propose a scheme where even a 3-step quantum walk can be unambiguously verified. This method is based on the fact that after each step of the quantum walk, along with the superposition of displacement, the particle also exists in a superposition of its internal states which is specific to the number of steps N of the quantum walk. At each position after an N-step quantum walk there is a probability for the particle to be found in state X and a probability for being in state Y. Summing over all positions, the probabilities of finding the particle in X and summing over all atoms, i, we get the total (unnormalized) probability $(P_X)_N = \Sigma_i \Sigma_k \langle \phi(k,X)|\Psi_N|\phi(k,X)\rangle_i$ of the atoms to be found in X after N steps of the quantum walk. Equivalently, this corresponds to the population of atoms in the state X after a N-step quantum walk in our system. Similarly, one may determine $(P_Y)_N$, the population in Y after N steps. It turns out that $(P_X)_N$ and $(P_Y)_N$ are indicative of N, the number of steps of the quantum walk that have been performed, especially for small N.

This is illustrated in Fig. 14 where $\frac{(P_X)_N}{n}$ [red (thin) lines] and $\frac{(P_Y)_N}{n}$ (blue/thick lines) are plotted as a function of N, with n being the total number of atoms and the initial population having all been in state X. If the Hadamard operation alone is performed without any accompanying displacement, the relative population of X and Y can acquire only the values 1.0 and 0.5 after application of any number of Raman $\pi/2$ pulses. In a quantum walk, alternating Hadamard and displacement operations cause interference of amplitudes giving rise to oscillations in the populations in the two states.

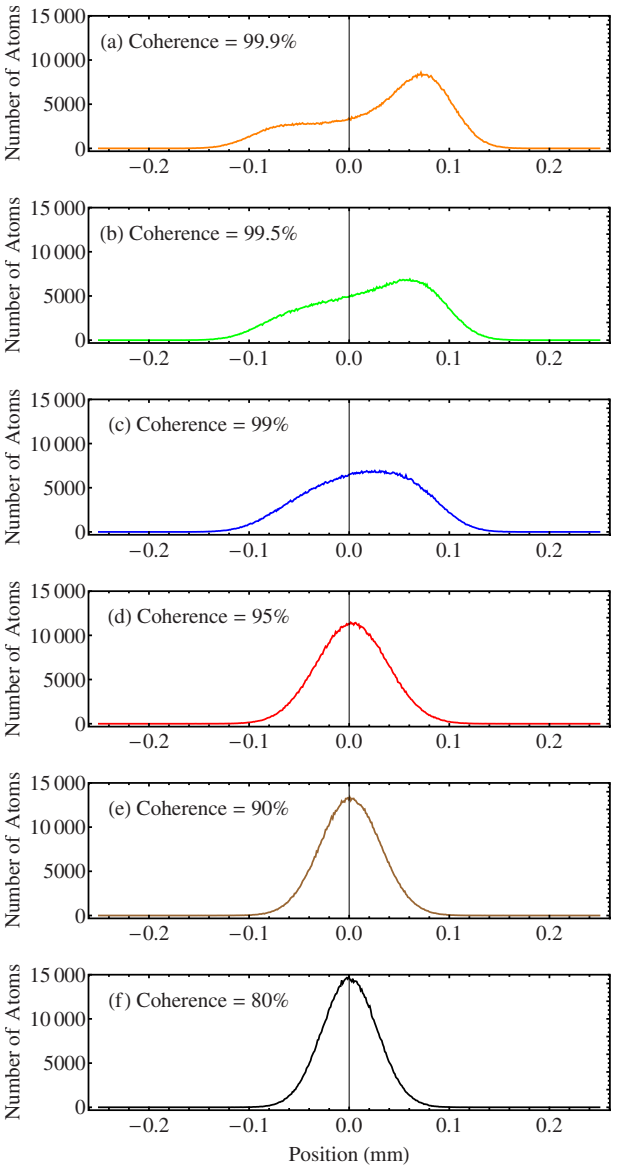

FIG. 13. (Color online). Simulated absorption signal for asymmetric walk of 250 steps for different coherences.

For a Hadamard walk starting with initial state X, the relative X population oscillates about 0.646 and the relative Y population about 0.354, with the amplitude of oscillation gradually decreasing. The difference in population $(P_X)_N$ and $(P_X)_{N+2}$ is most significant for smaller values of N making this method more suitable for few-step quantum walks. In an experiment such as ours individual atom events are probed in a bulk sample. Thus, the methods that seek to measure displacement in position space or momentum space, which are not bounded, require significant displacement before the distinction between classical random walk and quantum walk can be seen or even symmetric and antisymmetric quantum walks can be distinguished. If instead we measure in the space operated in by the Hadamard operator, where the limits are well defined, a measurement of population brings out the difference right at the third step. However, it should be noted that this method is only applicable to asymmetric quantum walks. For a symmetric quantum walk the relative population

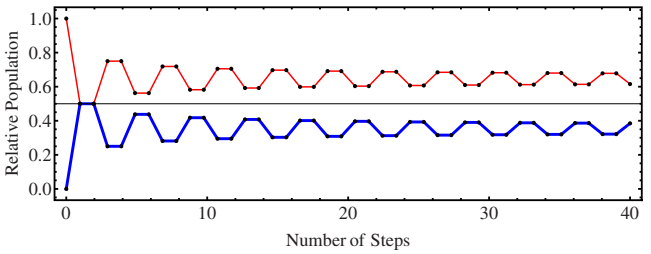

FIG. 14. (Color online). Population evolution of X state [red (thin) lines] and Y state (blue/thick lines) in a Hadamard walk starting with initial state X as a function of number of steps N. In both the cases, only the points are realizable values; they are joined by line segments as a guide to the eye.

of X and Y will always remain 0.5 as also in the case of classical random walk.

The strategy to adopt in order to detect the quantum walk would then be to initialize the atoms in the state X (or Y) and execute the walk for the required number of steps N by performing the sequence of operations $(DH)^N$. Two absorption measurements should then be carried out, one with the probe beam resonant with the X state and other resonant with the Y state, in order to determine the number of atoms in states X and Y. This gives the relative populations after N steps of the quantum walk. As the quantum walk is being carried out simultaneously by all atoms in the cold cloud, a single measurement of relative populations suffices. Second and more importantly, this measurement is independent of the size and the temperature of cold cloud.

The population evolution presented in Fig. 14 is for the ideal case of 100% fidelity. We now present the results for cases of inefficient displacement and reduced coherence. These are illustrated in Figs. 15 and 16 respectively. It can be seen that even for as low as 80% efficiency and 80% coherence up to 10 steps of quantum walks can be distinguished. The effect of reduced fidelity is very drastic in the case of relative population measurements as the number of steps increases. However, this sensitive dependence of relative population on efficiency may be used to test the coherence of a Hadamard walk before it is put to an application. By recording the steady state population of states X and Y for larger number of steps the presence or loss of coherence can be ascertained.

VII. DISCUSSION

We have established that a quantum walk can be performed and measured with cold atoms in a double optical lattice. We now point out some interesting features that may be tested out. The quantum walk is unitary and hence reversible. The Hadamard operation being the inverse of itself, merely the direction of the displacement has to be reversed to obtain an inverse quantum walk step. Applying the sequence $(DH)^{-1}=H^{-1}D^{-1}=HD^{-1}$, N times, we should obtain the original distribution, the limitations being inefficiencies and decoherence.

Decoherence is a very important consideration in the implementation of quantum walks. In a dilute collection of

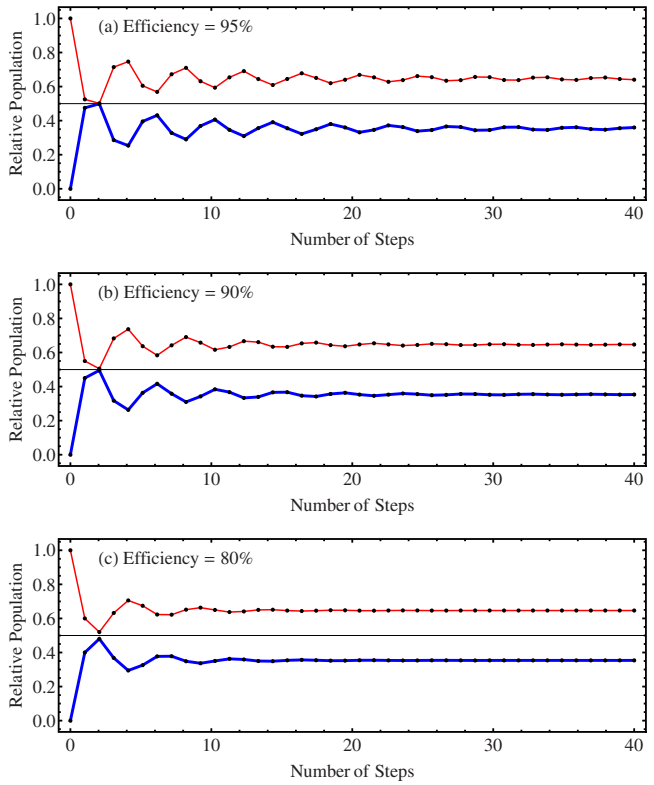

FIG. 15. (Color online). Population evolution of X state [red (thin) lines] and Y state (blue/thick lines) in a Hadamard Walk starting with initial state X as a function of number of steps N for different efficiencies of the displacement operator, (a) 95,(b) 90, and (c) 80%. In all cases, only the points are realizable values; they are joined by line segments as a guide to the eye.

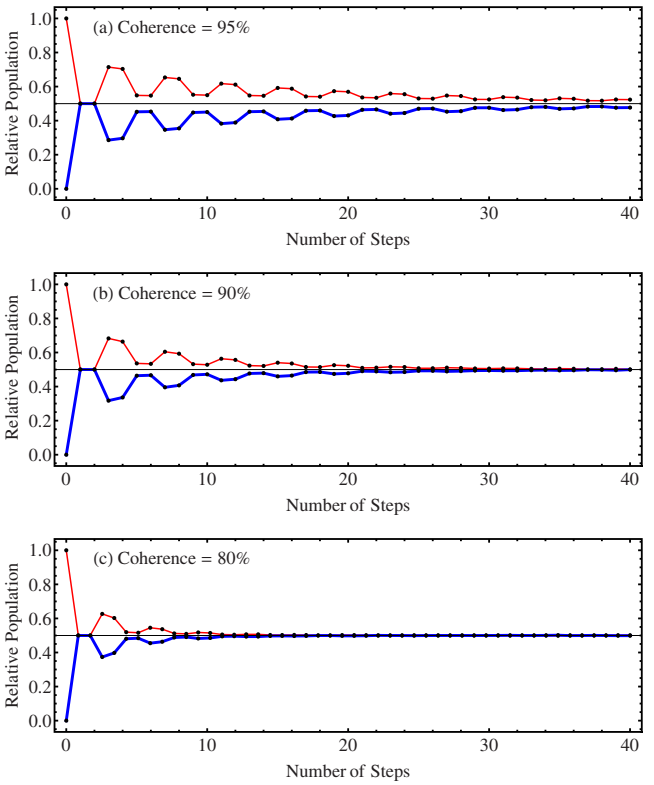

FIG. 16. (Color online). Population evolution of X state [red (thin) lines] and Y state (blue/thick lines) in a Hadamard Walk starting with initial state X as a function of number of steps N for different values of coherences, (a) 95, (b) 90, and (c) 80%. In all cases, only the points are realizable values; they are joined by line segments as a guide to the eye.

cold atoms, several factors limit the coherence apart from spontaneous emission during Raman pulse, e.g., scattering of the lattice beams and collisions of atoms. An increase in the number of steps increases delocalization of the wave function, thereby increasing the probability of collision between the atoms, and with it, their role in decoherence of the wave function. While increased delocalization will prove detrimental to a many step quantum walk, in the case of a few-step quantum walk, this may be used to study collisions and also to measure the relative roles of the various decohering effects. For example, a 100-step asymmetric quantum walk of 1 μm displacement per step and a 10-step asymmetric quantum walk of 10 μm will result in similar displacement to atoms and are unlikely to be distinguished in a displacement measurement of the quantum walk by absorption or time-of-flight techniques. However, as the population evolves as the number of steps of a quantum walk, independent of the step size, the two cases can be distinguished in a population measurement. By conducting, say, two 5-step quantum walks differing only in their step size, the observed difference in the population distributions can be attributed to decoherence due to collisions.

The relative displacement of the lattices in the envisaged experiment is to be carried out by an EOM. The EOM currently available is capable of inducing a relative spatial phase of up to 8π (four sites). This gives the possibility of having step lengths of one to four lattice sites. This however, need not limit the number of steps of the Hadamard walk; when limit of the EOM is reached, the population can be inverted by a π pulse, which swaps atoms from one lattice to the other. The spatial phase shift due to the EOM is then reduced from 8π back toward 0. As the populations have been inverted, this is equivalent to a continuation of the relative displacement of the original lattice in the original direction. The step length can also be increased by switching the displacement from the vertical to the horizontal direction, where the intersite distance is twice as large [26]. It is of importance that the translation is performed adiabatically, that is, the atoms have to be moved sufficiently slowly compared to their vibrational frequency, which is typically of the order of 100 kHz. The displacement can be carried out in any of the x,y,z directions opening up the possibilities of two- and three-dimensional quantum walks.

VIII. CONCLUSION

In summary, we have examined the feasibility of performing and detecting quantum walks in a collection of cold

atoms in a double optical lattice. We see that for present experimental capabilities, a few hundred steps of the quantum walks are required to see the two-peaked structure characteristic of one-dimensional quantum walks. We have shown that few-step asymmetric quantum walks can be detected and measured in cold atoms in optical lattices, if one measures the population of the internal states rather than the displacements.

[1] J. Kempe, Contemp. Phys. **44**, 307 (2003).
[2] A. M. Childs, R. Cleve, E. Deotto, E. Farhi, S. Gutmann, and D. A. Spielman, *Proceedings of the 35th ACM Symposium on Theory of Computing* (ACM Press, New York, 2003), p. 59.
[3] N. Shenvi, J. Kempe, and K. Birgitta Whaley, Phys. Rev. A **67**, 052307 (2003).
[4] A. M. Childs and J. Goldstone, Phys. Rev. A **70**, 022314 (2004).
[5] A. Ambainis, J. Kempe, and A. Rivosh, *Proceedings of ACM-SIAM Symposium on Discrete Algorithms (SODA)* (SIAM, Philadelphia, 2005, pp. 1099.
[6] M. Hillery, J. Bergou, and E. Feldman, Phys. Rev. A **68**, 032314 (2003).
[7] Z. Zhao, J. Du, H. Li, T. Yang, Z.-B. Chen, and Jian- Wei Pan, e-print arXiv:quant-ph/0212149.
[8] P. L. Knight, E. Roldan, and J. E. Sipe, Opt. Commun. **227**, 147 (2003).
[9] X. Zou, Yuli Dong, and Guangcan Guo, New J. Phys. **8**, 81 (2006).
[10] B. C. Travaglione and G. J. Milburn, Phys. Rev. A **65**, 032310 (2002).
[11] W. Dur, R. Raussendorf, V. M. Kendon, and H. J. Briegel, Phys. Rev. A **66**, 052319 (2002).
[12] C. M. Chandrashekar, Phys. Rev. A **74**, 032307 (2006).
[13] K. Eckert, J. Mompart, G. Birkl, and M. Lewenstein, Phys. Rev. A **72**, 012327 (2005).
[14] T. Di, M. Hillery, and M. S. Zubairy, Phys. Rev. A **70**, 032304 (2004).
[15] G. S. Agarwal and P. K. Pathak, Phys. Rev. A **72**, 033815 (2005).
[16] B. C. Sanders, S. D. Bartlett, B. Tregenna, and P. L. Knight, Phys. Rev. A **67**, 042305 (2003).
[17] R. Cote, A. Russell, E. E. Eyler, and P. L. Gould, New J. Phys. **8**, 156 (2006).
[18] E. Farhi and S. Gutmann, Phys. Rev. A **58**, 915 (1998).
[19] J. Du, H. Li, X. Xu, M. Shi, J. Wu, X. Zhou, and R. Han, Phys. Rev. A **67**, 042316 (2003).
[20] C. A. Ryan, M. Laforest, J. C. Boileau, and R. Laflamme, Phys. Rev. A **72**, 062317 (2005).
[21] B. Do, M. L. Stohler, S. Balasubramanian, D. S. Elliot, C. Eash, E. Fischbach, M. A. Fischbach, A. Mills, and B. Zwickl, J. Opt. Soc. Am. B **22**, 499 (2005).
[22] P. Zhang, X.-F. Ren, X.-B. Zou, B.-H. Liu, Y.-F. Huang, and G.-C. Guo, Phys. Rev. A **75**, 052310 (2007).
[23] H. B. Perets, Y. Lahini, F. Pozzi, M. Sorel, R. Morandotti, and Y. Silberberg, Phys. Rev. Lett. **100**, 170506 (2008).
[24] D. A. Steck, http://steck.us/alkalidata/cesiumnumbers.pdf
[25] H. Ellmann, J. Jersblad, and A. Kastberg, Phys. Rev. Lett. **90**, 053001 (2003).
[26] H. Ellmann, J. Jersblad, and A. Kastberg, Eur. Phys. J. D **22**, 355 (2003).
[27] P. Jessen and I. Deutsch, Adv. At., Mol., Opt. Phys. **37**, 95 (1996).
[28] G. Grynberg and C. Robilliard, Phys. Rep. **355**, 335 (2001).
[29] P. Sjölund, S. J. H. Petra, C. M. Dion, S. Jonsell, M. Nylén, L. Sanchez-Palencia, and A. Kastberg, Phys. Rev. Lett. **96**, 190602 (2006).
[30] H. Ellmann, J. Jersblad, and A. Kastberg, Eur. Phys. J. D **13**, 379 (2001).
[31] J. Jersblad, H. Ellmann, and A. Kastberg, Phys. Rev. A **62**, 051401(R), (2000).
[32] P. D. Lett, R. N. Watts, C. I. Westbrook, W. D. Phillips, P. L. Gould, and H. J. Metcalf, Phys. Rev. Lett. **61**, 169 (1988).
[33] H. Hagman, P. Sjölund, S. J. H. Petra, M. Nylén, A. Kastberg, H. Ellmann, and J. Jersblad, J. Appl. Phys. **105**, 083109 (2009).